Novel active noise-reducing headset using earshell vibration control

Boaz Rafaely,[a] Joao Carrilho, and Paolo Gardonio
Institute of Sound and Vibration Research, University of Southampton, Southampton SO17 1BJ, United Kingdom

(Received 24 September 2001; revised 3 July 2002; accepted 6 July 2002)

Active noise-reducing (ANR) headsets are available commercially in applications varying from aviation communication to consumer audio. Current ANR systems use passive attenuation at high frequencies and loudspeaker-based active noise control at low frequencies to achieve broadband noise reduction. This paper presents a novel ANR headset in which the external noise transmitted to the user's ear via earshell vibration is reduced by controlling the vibration of the earshell using force actuators acting against an inertial mass or the earshell headband. Model-based theoretical analysis using velocity feedback control showed that current piezoelectric actuators provide sufficient force but require lower stiffness for improved low-frequency performance. Control simulations based on experimental data from a laboratory headset showed that good performance can potentially be achieved in practice by a robust feedback controller, while a single-frequency real-time control experiment verified that noise reduction can be achieved using earshell vibration control. © *2002 Acoustical Society of America.* [DOI: 10.1121/1.1504469]

PACS numbers: 43.50.Ki, 43.50.Hg, 43.66.Vt [MRS]

I. INTRODUCTION

Active noise-reducing (ANR) headsets are used to protect the ear from overexposure to noise, in situations where the passive circumaural headset does not provide, by itself, sufficient reduction in the noise level. Active attenuation, usually dominant at low frequencies, is complemented by passive attenuation at high frequencies to produce improved overall noise reduction performance. ANR headsets are widely used in aviation and military communication and in noisy industrial environments, and are one of the most commercially successful applications of the active noise control technology.

ANR headsets which employ a loudspeaker and a microphone inside the earshell connected via an analog feedback controller were studied in the 50's by Meeker, Hawley, and Simshauser.[1–3] Wheeler[4] studied the design of ANR headset for aviation communication, while Bai and Lee[5] proposed the use of modern controller design techniques for the ANR system. Recent studies proposed the use of digital systems to improve performance.[6–8] The ANR headsets described above and those currently used in commercial applications employ active attenuation by using a loudspeaker to produce the antinoise at the low frequencies, therefore reducing the noise level at the user's ear. Current active headsets could benefit from further improvements, particularly when operating in severe environments, by increasing sound attenuation and by improving mechanical robustness.

This paper proposes a novel approach to ANR headsets,[9] which can be applied as an alternative or as a complement to conventional systems, and which has the potential for improving both performance and mechanical robustness through the use of vibration transducers. Instead of generating sound inside the headset earshell using a loudspeaker, the noise level at the ear is reduced by attenuating the vibration transmission through the shell, using vibration actuators. The vibration actuator is attached to the earshell and produces a force that opposes the force imposed by the external noise, therefore reducing earshell vibration. An accelerometer mounted on the earshell can be used as a control sensor. At relatively low frequencies where the coupled response of the earshell and acoustic cavity could be modeled to be equivalent to that of a lumped mass (the earshell) connected to two lumped springs (the headset cushion and the air in the cavity),[10] the proposed control approach can be regarded as a typical active vibration isolation problem as described by Fuller *et al.*[11] in Chap. 7.2. At higher frequencies, where the sound transmission is controlled by the coupling of the earshell modes with the cavity modes, the proposed control approach should be regarded as a special case of active structural acoustic control (ASAC) as presented by Fuller *et al.*[11] in Chap. 9.

This paper presents a theoretical analysis of the new ANR headset, supplemented by simulations and an experimental study using a laboratory ANR headset system.

II. HEADSET SYSTEM MODELING

This section presents a model-based theoretical analysis of the ANR headsets studied in this paper. The models are later used to study performance with velocity feedback control. Since the ANR headsets described in this paper are designed around a passive noise-reducing headset,[10] this section starts with a brief description of a passive headset, followed by modeling of an active headset which uses ideal secondary force, and more practical secondary forces generated by force actuators. The first actuator is connected between the earshell and an inertial mass, and is therefore re-

[a]Electronic mail: br@isvr.soton.ac.uk

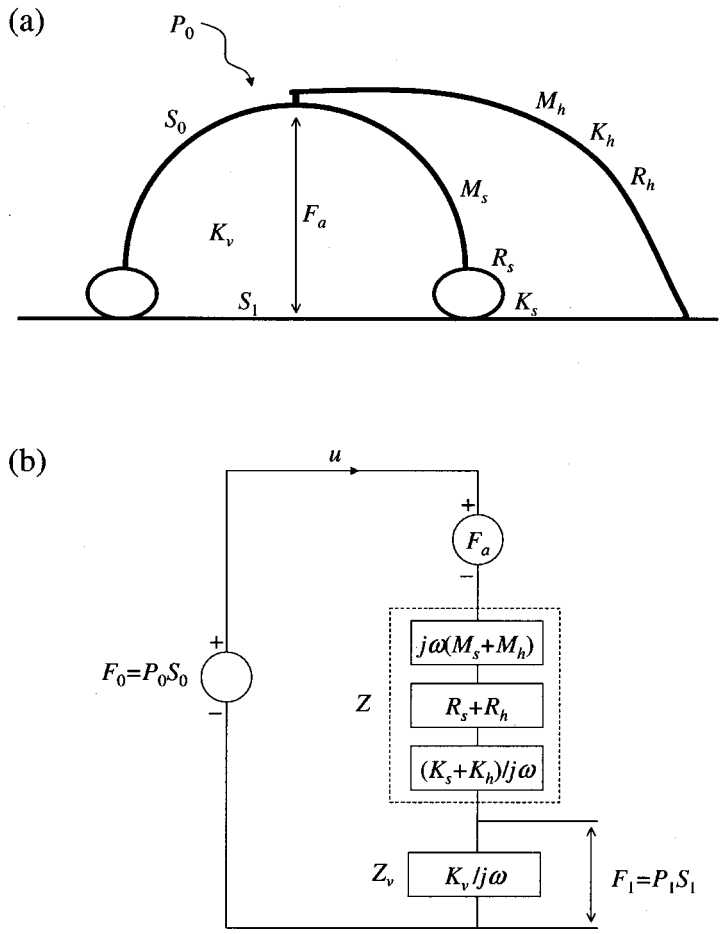

FIG. 1. (a) Schematic diagram of the headset system, and (b) an equivalent impedance block diagram.

ferred to as an inertial actuator, and the second actuator is mounted between the earshell and the headband, and is referred to as a headband force actuator.

Lumped-element models previously used by Shaw and Thiessen[10] provide a simple representation of the underlying systems' dynamics, and are used here to analyze the combined passive–active headset systems. The model provides good approximation of system performance at the low-frequency range, where the acoustic wavelength is larger than the earshell dimensions.

It should be noted that the simplified physical model is employed here to study potential performance and the suitability and limitations of the actuator, and provides an insight to the behavior of the system. It is not suggested as a model from which a practical controller could be designed. The measured headset response is used for the latter, as presented in Sec. IV.

A. Passive headset

The sound transmission in noise-reducing headsets has been found to be similar to the vibration transmission in a mass–spring–damper system.[10] Figure 1(a) shows an idealized headset earshell consisting of a rigid earshell of mass M_s, sealed by a cushion of stiffness K_s and damping R_s to a rigid surface representing the head. The earshell is allowed to move only in the plane perpendicular to the surface, and the external noise, represented by the sound pressure P_0, is transmitted into the earshell inner volume through the earshell movements, assuming no leaks exist in the sealing of the earshell to the head. The earshell is assumed to be held in place by a headband, which has a mass M_h, stiffness K_h, and damping R_h. The mechanical impedance diagram shown in Fig. 1(b) was developed to represent the headset system,[10] with F_0 denoting the external force applied by the external acoustic pressure P_0 over the external earshell area S_0, and F_1 denoting the force applied inside the earshell volume by the inner pressure P_1, with S_1 the area enclosed by the cushion. In the case of the passive headset described here, it is assumed that the secondary force F_a in Fig. 1 is zero. From the diagram in Fig. 1(b), an expression for the sound transmission P_1/P_0 can be calculated as

$$\frac{P_1}{P_0}=\frac{S_0}{S_1}\frac{Z_v}{Z_v+Z}=\frac{S_0}{S_1}\frac{K_v}{K_v+K_s+K_h+j\omega(R_s+R_h)-\omega^2(M_s+M_h)}, \tag{1}$$

where $K_v=\rho c^2 S_1^2/V$ is the stiffness of the air volume V enclosed by the earshell, which is interacting with the earshell mass over the area S_1, and ρ and c are the air density and speed of sound, respectively. Equation (1) describes the transmission of a second order system with a resonance frequency at

$$\omega_0 = \sqrt{\frac{K_S + K_v + K_h}{M_S + M_h}}. \tag{2}$$

At frequencies below the resonance, the transmission reduces to

$$\frac{P_1}{P_0} = \frac{S_0}{S_1} \frac{K_v}{K_v + K_s + K_h}, \tag{3}$$

and the transmission magnitude is controlled solely by the stiffness of the headband, cushion, and the volume of air inside the earshell. Larger internal volume and larger cushion and headband stiffness will increase the noise attenuation at the lower frequencies.

B. Active headset with ideal secondary force

The vibration of the headset earshell can be reduced by introducing a secondary force which opposes the force generated by the external sound field. This will then reduce the sound developed inside the earshell volume, and therefore the sound preceived by the user. In this section it is assumed that a secondary force can be applied to the earshell, in an ''ideal'', way, where the dynamics of potential actuators is not taken into account. The latter is introduced later in this section. The force F_a in Fig. 1(a) represents an ideal control force, acting between the earshell and the rigid surface. The sound pressure inside the earshell volume, P_1, can be expressed using Fig. 1(b) as the superposition of the contributions of the two sources

$$P_1 = AP_0 + BF_a, \tag{4}$$

where A and B are given by

$$A = \frac{S_0}{S_1} \frac{Z_v}{Z_v + Z}, \quad B = -\frac{1}{S_1} \frac{Z_v}{Z_v + Z}. \tag{5}$$

The optimal arrangement for completely canceling the sound transmission can be calculated from Eqs. (4) and (5) by setting P_1 to zero, which produces an optimal secondary force of $F_a = P_0 S_0$. This can be implemented in practice by feeding the signal from an external reference microphone measuring P_0, to the input of a control actuator generating F_a, in a feedforward control arrangement. The latter will provide good broadband performance if the delay of the controller is sufficiently small.[12] Although this approach could potentially provide a control solution, it is not studied in this work, but suggested for future study.

The control approach considered in this paper is feedback control, where velocity feedback is initially studied due to its simplicity and potential to provide both good performance and stability when used to actively increase damping.[11] Using the earshell velocity u to feed F_a, such that $F_a = -gu$, where g is a gain constant with units of Ns/m, and writing u as F_1/Z_v, the sound transmission with velocity feedback can be written using Eq. (4) as

$$\frac{P_1}{P_0} = \frac{A}{1 + \frac{gS_1}{Z_v} B}. \tag{6}$$

C. Active headset with inertial force actuator

An inertial actuator can be modeled at low frequencies by a lumped mass–spring system, composed of the inertial mass M_a and the stiffness K_a of the force actuator. The inertial actuator, when mounted on the earshell system, as shown in Fig. 2(a), becomes what is known as a tuned vibration neutralizer,[13] and is most effective in reducing the earshell vibration at the resonance frequency of the inertial actuator system, $\omega_a = \sqrt{K_a/M_a}$. It should be noted that M_a denotes the inertial mass, while the mass of the actuator itself, including casing and transduction elements, are not considered separately but can be lumped into the earshell mass. Figure 2(b) shows the impedance diagram developed for this system. Assuming velocity feedback control is applied here as described above, Eq. (6) also applies here, and A and B can be found by superposition of the primary and secondary sources as

$$\begin{aligned} A &= \frac{S_0}{S_1} \frac{Z_v}{Z + Z_v + Z_{Ka} \| Z_{Ma}}, \\ B &= -\frac{1}{S_1} \frac{Z_{Ma} \| (Z + Z_v)}{Z_{Ka} + Z_{Ma} \| (Z + Z_v)} \frac{Z_v}{Z + Z_v}, \end{aligned} \tag{7}$$

where the notation $Z_1 \| Z_2$ denotes a parallel connection of impedances, calculated as $Z_1 Z_2/(Z_1 + Z_2)$.

D. Active headset with force actuator attached to the headband

An alternative to the inertial actuator described above is to mount the force actuator between the earshell mass and the headband, allowing the force actuator to react against the headband rather than the inertial mass, M_a. The latter is assumed to be removed from the actuator before mounting and is not used in this configuration, while the mass of the actuator itself is lumped into the earshell mass as described above. The advantage of this configuration, which is illustrated in Fig. 3(a), is that it does not require the additional mass used by the inertial actuator, which increases the overall weight of the headset, therefore compromising comfort and imposing a phase shift,[14] therefore potentially compromising control performance. In this arrangement, the headband impedance, Z_h, composed of the headband stiffness K_h, mass M_h, and damping R_h, is separated from the earshell impedance Z_s due to the mounting of the actuator between the heaband and the earshell. Figure 3(b) shows the impedance diagram for this arrangement. Similar to the case of the inertial actuator presented above, the transmission of sound through the earshell can be calculated from Eq. (6), with A and B given by

$$\begin{aligned} A &= \frac{S_0}{S_1} \frac{Z_v}{Z_s + Z_v + Z_{Ka} \| Z_h}, \\ B &= -\frac{1}{S_1} \frac{Z_h \| (Z_s + Z_v)}{Z_{Ka} + Z_h \| (Z_s + Z_v)} \frac{Z_v}{Z_s + Z_v}. \end{aligned} \tag{8}$$

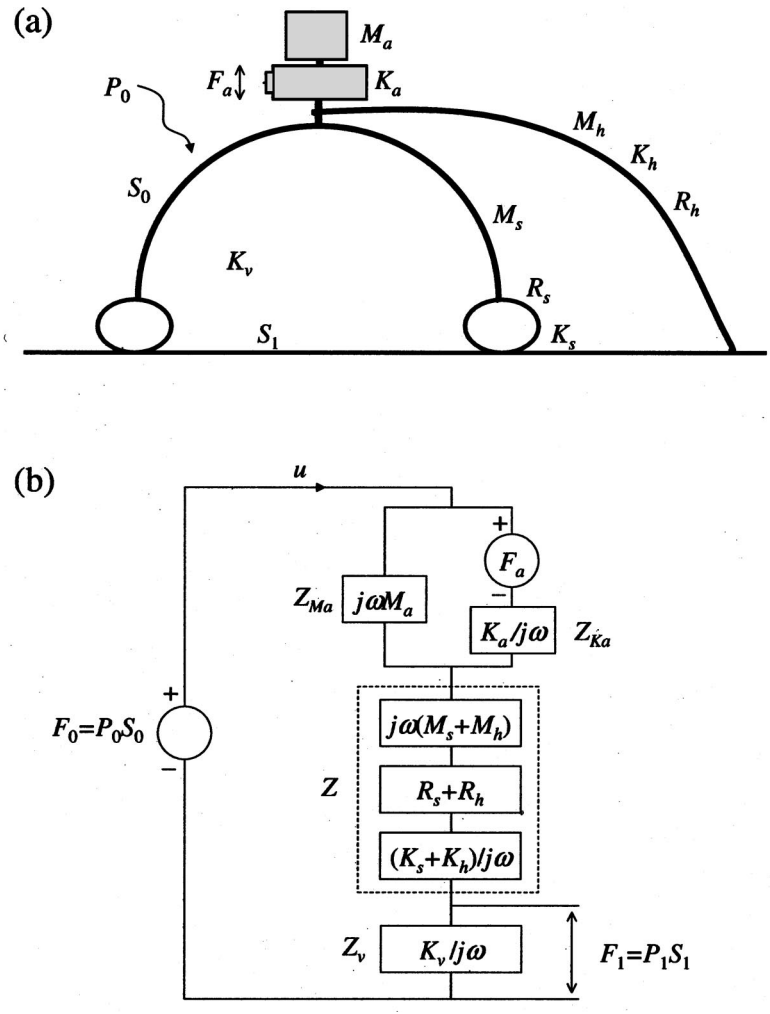

FIG. 2. (a) Schematic diagram of the active headset system with an inertial force actuator, and (b) an equivalent impedance block diagram.

III. VELOCITY FEEDBACK CONTROL SIMULATIONS USING HEADSET MODELS

The models developed above for the active headset are used in this section to simulate noise reduction performance and the force and displacement requirements from the actuator in the various configurations. Velocity feedback control is studied due to its simplicity and since it has shown to produce good performance with large stability margins in other applications by increasing the system damping.[11] This section starts by verifying the model of a commercial passive noise-reducing headset at the low frequencies, and then simulating control performance for the various active headset configurations.

A. The passive noise-reducing headset

The control simulations in this section use the headset model presented above, with the parameters taken from a commercial light-weight passive noise-reducing headset, manufactured by JSP, model KMO7236. Most of the headset parameters have been estimated from measurements, while some parameters, such as the damping of the earshell cushion, have been estimated by fitting the attenuation curve to manufacturer's data. The parameters and their values are listed in Table I. Figure 4 presents the passive transmission of sound through the headset, or passive attenuation, as calculated using Eq. (1) compared to manufacturer's data, showing good agreement at the lower frequencies. Since high-frequency acoustical and mechanical system dynamics were not included in the model, the attenuation is not predicted accurately at the high-frequency range. Nevertheless, the simplified model provides an insight into the behavior of the system and can be used to analyze performance at the low frequencies, which is normally the frequency range of interest for active control.

B. Control with ideal secondary force

Figure 5(a) shows a plot of the transmission P_1/P_0 for the passive system described in Fig. 1(a) and calculated using Eq. (1) and Table I, and for the active system with velocity feedback control and an ideal secondary force calculated using Eq. (6). The effect of velocity feedback is to increase the damping of the system, and indeed the active attenuation is increased mostly around the resonance frequency of the passive system. Figure 5(b) shows the Nyquist diagram for the open-loop system with velocity feedback control, with the gain parameter g set to -2900. The curve is completely in the positive-real quadrants, which gives this type of feedback control the advantage of large stability margins.[11] In practice, however, actuators must be used to produce the secondary force, and so control simulations with the two actuator configurations are presented next.

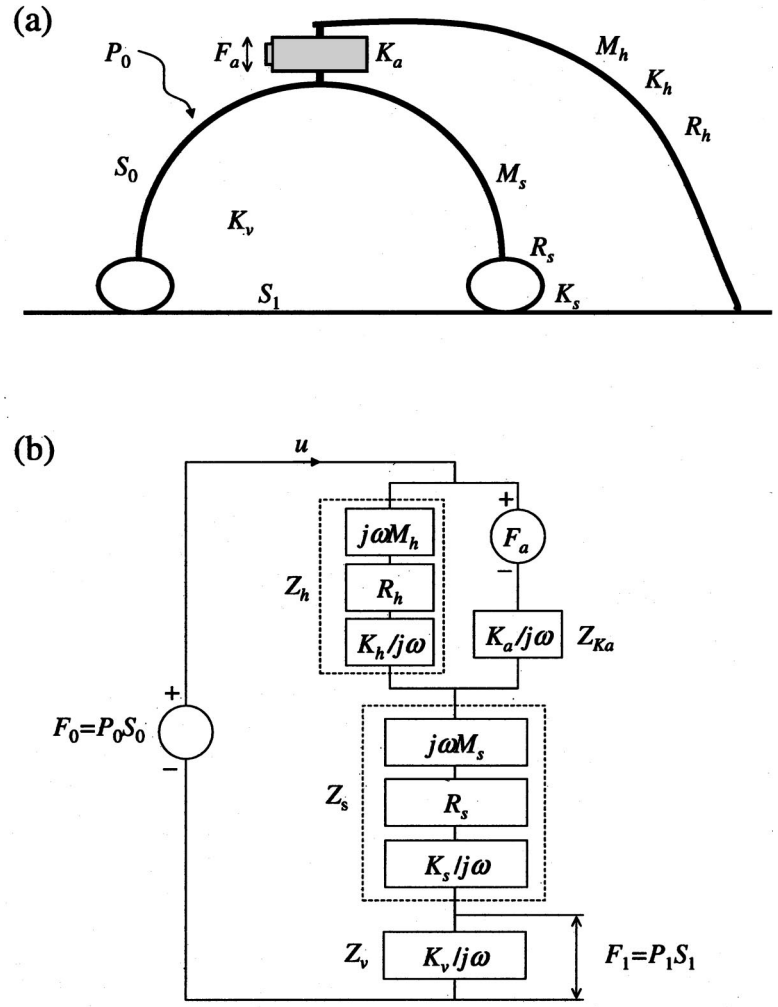

FIG. 3. (a) Schematic diagram of the active headset system with a force actuator fitted between the earshell and the headband, and (b) an equivalent impedance block diagram.

C. Control with inertial force actuator

Control simulations with an inertial force actuator attached to the earshell are presented in this section. Figure 6(a) shows simulations of the sound transmission for the original passive system calculated using Eq. (1); the active system with no control, calculated using Eqs. (6) and (7) and $g=0$; and the active system with control, calculated using Eqs. (6) and (7) and $g=-305$. The parameters for the inertial force actuator are presented in Table II, which represents a PCB 712A02 force actuator. This force actuator was chosen since it is mechanically robust, can produce relatively large forces, and is designed to work in the low-frequency range, i.e., 150 to 500 Hz according to its specifications.

TABLE I. JSP KMO7236 headset parameters.

Parameter	Value	Description
M_s	77 g	Earshell mass
K_s	$7\cdot10^4$ N/m	Cushion stiffness
R_s	90 Ns/m	Cushion damping
M_h	8 g	Headband effective mass
K_h	50 N/m	Headband stiffness
R_h	5 Ns/m	Headband damping
V	180 cc	Earshell cavity volume
S_0	79 cm^2	Outer earshell area
S_1	25 cm^2	Inner earshell area

The effect of mounting the inertial actuator is to provide additional attenuation around its resonance frequency, i.e., 250 Hz, with an increase in transmission above the resonance frequency. The resonance frequency of the earshell around 100 Hz is also decreased due to the added inertial mass of 150g.

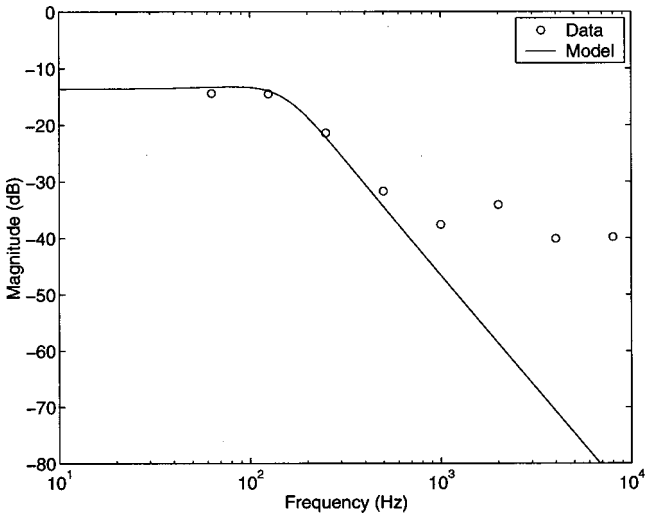

FIG. 4. Passive attenuation of the headset as simulated using Eq. (1) compared to manufacturer's data.

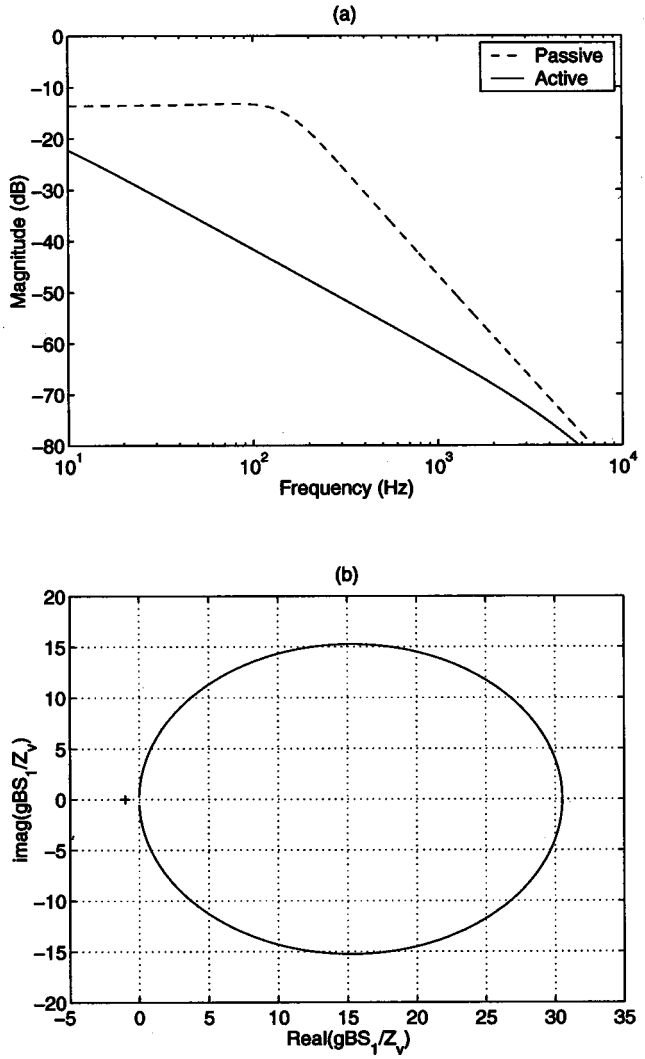

FIG. 5. (a) Theoretical comparison of sound transmission between the passive headset and an active system with an ideal secondary force, and (b) the corresponding Nyquist diagram of the open-loop response of the active system.

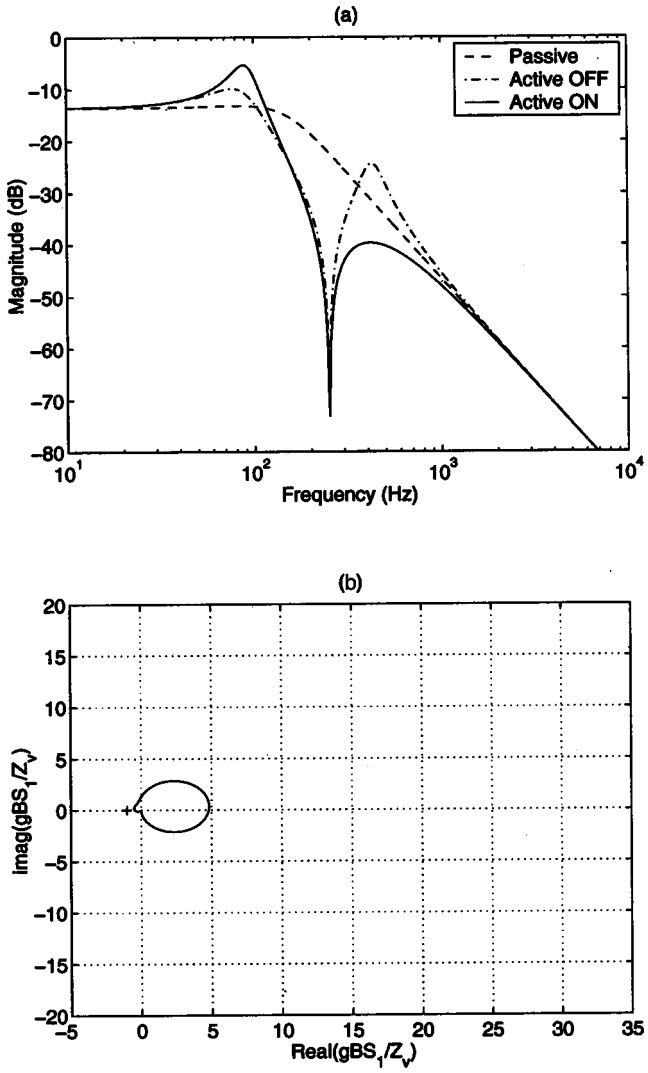

FIG. 6. (a) Theoretical comparison of sound transmission between the passive headset and an active system with an inertial actuator, and (b) the corresponding Nyquist diagram of the open-loop response of the active system.

Once control is applied, the transmission is attenuated above the actuator resonance frequency, and slightly enhanced at the earshell resonance frequency. The latter can be explained by Fig. 6(b), which shows the Nyquist plot for the inertial actuator system. Although the curve is mostly on the right-hand side and therefore provides good stability, it has a small negative real part corresponding to the low-frequency enhancement. An inertial actuator with a lower resonance frequency will produce attenuation at a lower frequency range, with amplification at an even lower frequency, which will be more useful in practice. Such an actuator, however, will require large inertial mass and low stiffness, making it less attractive in practice.

The analysis presented here showed that the dynamics of the actuator system could impose a limit on performance, if stability is to be maintained.

D. Control with a headband force actuator

The sound transmission of the active headset with a force actuator attached between the earshell and the headband is simulated in this section. Figure 7(a) shows the simulated sound transmission for the passive system; the active system with no control, calculated using Eqs. (6) and (8) and $g=0$; and the active system with control, calculated using Eqs. (6) and (8) and $g=-1600$. As above, the parameters for the headset and actuator are presented in Tables I and II. The mounting of the actuator has a small effect on the sound transmission, while the highest active attenuation is observed above the mounted resonance frequency, which is around 1 kHz. Figure 7(b) shows that stability margins in this case are larger compared to the inertial actuator configuration in Fig.

TABLE II. PCB 712A02 force actuator parameters.

Parameter	Value	Description
M_a	150 g	Actuator inertial mass
K_a	$3.7\cdot 10^5$ N/m	Actuator stiffness
f_{0_a}	250 Hz	Resonance frequency
F_{cl}	6.7 N	Clamped force (peak)
X_{fr}	6.5 μm	Free displacement (peak)

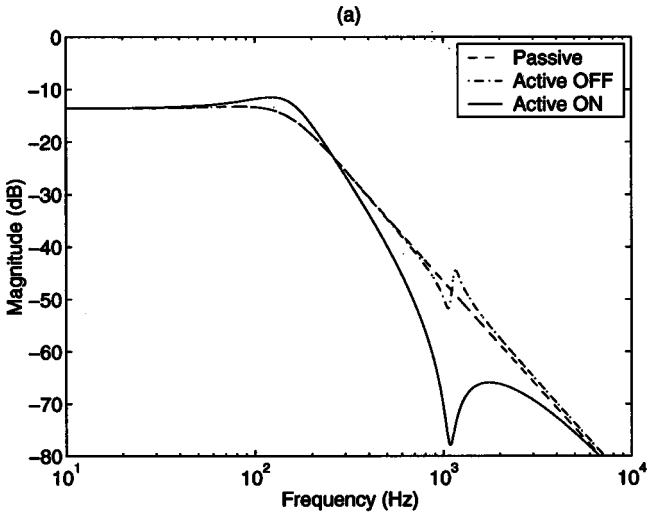

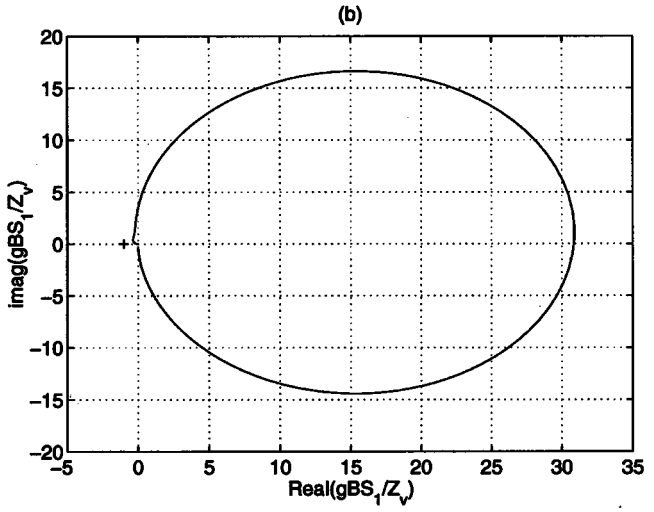

FIG. 7. (a) Theoretical comparison of sound transmission between the passive headset and the active system with the actuator fitted between the earshell and the headband, and (b) the corresponding Nyquist diagram of the open-loop response of the active system.

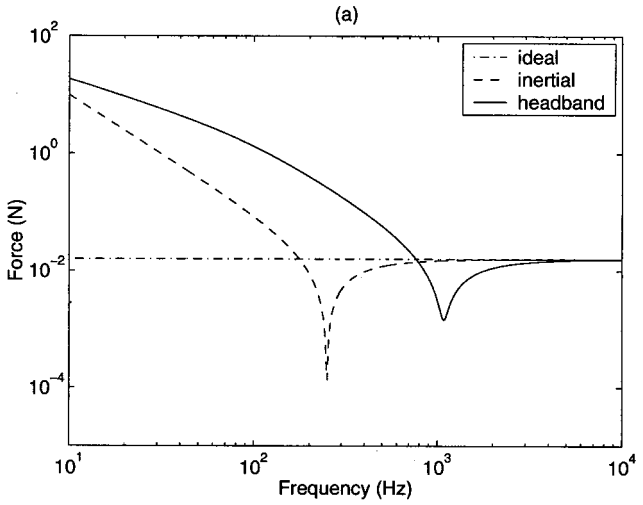

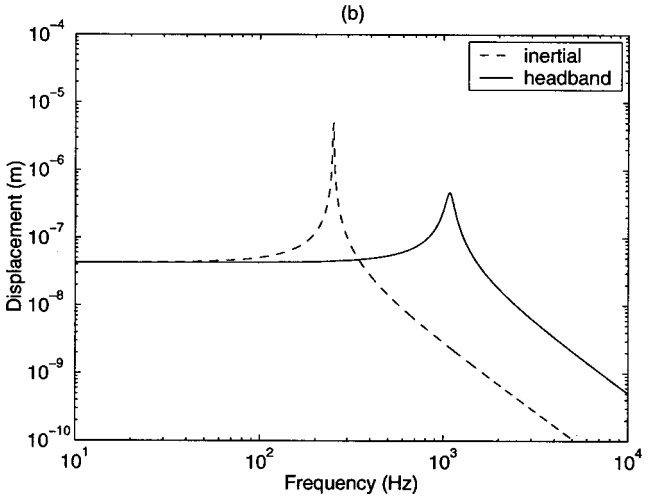

FIG. 8. (a) Force required to completely cancel 100-dB SPL noise, with three secondary source configurations: ideal, inertial actuator, and headband actuator, and (b) actuator displacement, or stroke, required to completely cancel 100-dB SPL noise, with two secondary source configuration: inertial actuator, and headband actuator. Note that displacement is zero for the ideal source case.

6(b). Nevertheless, an actuator with a smaller stiffness will be required to produce attenuation at a lower frequency range to better complement the passive attenuation.

E. Control forces and actuator displacement

The simulation presented above showed that an actuator with lower stiffness is required if active attenuation is to be achieved at the low-frequency range, i.e., below 1 kHz. Other important actuator parameters are the force and displacement required to cancel the primary disturbance. These are evaluated here using simulations with a primary noise of 100 dB SPL. Assuming the pressure inside the earshell in Eq. (4) is completely canceled, the corresponding optimal control force is given by

$$F_{a_{\text{opt}}} = -\frac{AP_0}{B}. \tag{9}$$

Figure 8(a) shows the optimal control force for the three control configurations of an ideal source, inertial actuator, and headband actuator. A constant force is required in the ideal source case, while a higher force is required from the actuators at low frequencies in the other two configurations due to the relatively low impedance of the supporting inertial mass and headband. Lower forces are required around the mounted actuator resonance frequencies.

The optimal force cancels the primary disturbance and therefore reduces the displacement of the earshell to zero. The ''actuator'' displacement, or stroke, in the ideal source case is therefore zero. The actuator stroke in the inertial actuator configuration can therefore be calculated by setting the velocity u to zero in Fig. 2(b), as

$$X_{a_{\text{opt}}} = -\frac{1}{j\omega}\frac{F_{a_{\text{opt}}}}{Z_{M_a}+Z_{K_a}}, \tag{10}$$

and for the headband actuator using Fig. 3(b) as

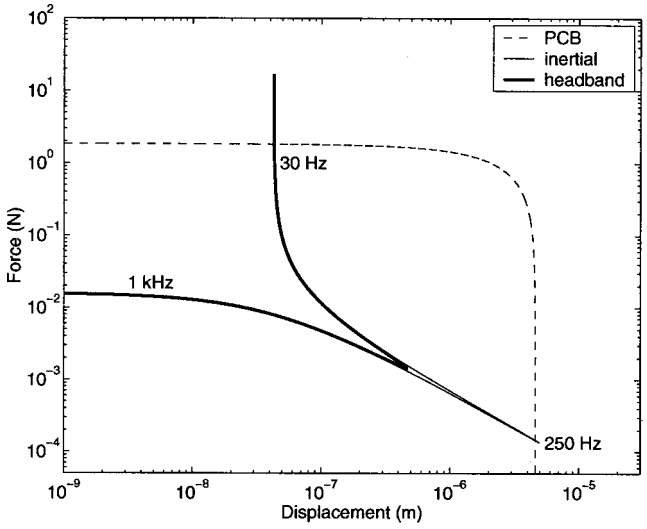

FIG. 9. The maximum force and actuator displacement, or stroke, provided by the actuator, compared to force and stroke required to cancel external noise of 100 dB SPL in the two actuator configurations.

$$X_{a_{\text{opt}}} = -\frac{1}{j\omega}\frac{F_{a_{\text{opt}}}}{Z_h + Z_{K_a}}. \tag{11}$$

Figure 8(b) shows that the stroke required from the actuators is highest around the mounted resonance frequencies.

The next simulation is used to investigate whether the force and stroke required to cancel 100-dB SPL noise, as calculated above, can be produced by the PCB actuator described in Table II. The relation between the maximum force produced by the actuator for a given displacement is assumed to behave linearly,[15] and is calculated from the clamped force and free displacement provided in Table II. This is then compared to the actual force and stroke required as calculated above. Figure 9 shows the maximum force vs actuator displacement, or stroke, provided by the PCB actuator compared to the required values. Some frequency values of the force and displacement pairs are also denoted. At most of the working frequency range the required force and displacement are within the actuator limits, except at very low frequencies, where the force required is slightly higher than the force available, for both actuator configurations. Also, at the resonance frequency of the inertial actuator system, the displacement required is slightly higher than the actuator limit. Overall, at most of the working range, the PCB actuator considered can provide the required force and stroke to cancel an external noise of 100 dB SPL.

If the level of the surrounding primary noise is higher than 100 dB SPL, e.g., near very noisy machines or engines, the limitation imposed by this actuator might compromise performance. In this case an improved actuator is required. The design of such an actuator is suggested for future work.

IV. ROBUST CONTROL SIMULATIONS USING MEASURED DATA

A simulation study using data measured on a laboratory active headset system was performed to investigate the potential performance of the active headset in practice. First, measurements were obtained from the laboratory active headset. Then, the measured data were used to design a controller and simulate its performance and robustness. The setup, and measurement and simulation results are presented in this section.

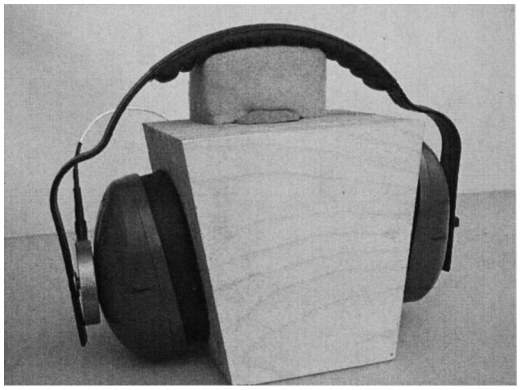

FIG. 10. A photo of the active headset with the PCB actuator mounted between the earshell and the headband.

A. Setup

A laboratory active headset has been constructed and control simulations have been performed using data measured from the laboratory headset. The experimental active headset included a passive JSP noise-reducing headset, mounted on a wooden block with dimensions of an average human head. One electret microphone was mounted inside the earshell, and one outside. A PCB type 712A02 piezoelectric force actuator was mounted on the earshell in the two configurations, i.e., as an inertial actuator with an inertial mass of 150 g, and between the headband and earshell, as illustrated in Figs. 2(a) and 3(a), and was driven by an AVL power amplifier model 790. A Bruel & Kjaer accelerometer type 4375 connected to a charge amplifier type 2635 was mounted on the earshell, colocated with the actuator, and measured earshell velocity. The measurements were recorded using an Advantest R9211C FFT analyzer, and used in the control simulations. A photo of the headset with the PCB actuator mounted between the earshell and the headband is shown in Fig. 10.

B. Control with inertial force actuator

The performance of the active headset system with the inertial actuator was investigated in this section using simulations with data measured on the laboratory system. The acoustic transmission between the external and internal microphones denoted by A was measured by introducing broadband noise through an external loudspeaker. The response between the voltage input to the force actuator's amplifier and the velocity output measured by the accelerometer's charge amplifier, denoted by H, was also measured. Then, a feedback controller with a frequency response C was designed to control the plant H, as described below. It is assumed that the reduction in the earshell vibration due to the control, denoted by $1/(1+CH)$, is proportional to the reduction in the sound transmission, and so the latter with active control can be calculated by

$$\frac{P_1}{P_0} = \frac{A}{1+CH}. \tag{12}$$

Initial control simulation employed a constant velocity-feedback control filter C. The performance of the active headset was very poor due to high-frequency dynamics of the active headset system, which generated negative-real values in the Nyquist open-loop response. The model-based simulations in Sec. III, which showed good performance using velocity feedback, didn't include the system's high-frequency acoustic and structural dynamics, and so when these were included in the measured headset response, the constant gain controller provided poor performance if it was to maintain stability. A feedback controller was therefore designed using an internal model control (IMC) configuration,[16] with a finite impulse response (FIR) control filter with 256 coefficients, and a sampling rate of 20 kHz. The controller was designed to minimize the mean-square vibration signal at the control frequency range, but was made robust for multiplicative uncertainties of 100%,[17,18] which guaranteed stability for any deviation smaller than 6 dB of the plant response from the measured response used in the design.

It should be noted that the aim of the study in this section is to show potential performance with a feedback control filter, and so other feedback controller design methods could have been used (e.g., H_∞ control[19]). Also, the plant uncertainty value of 100% was introduced to provide some robustness in the design. It is clear that a more comprehensive study of the system's response and its variability are required for the design of a controller that is to be implemented in practice. This is, however, suggested for future work.

Figure 11(a) shows the sound transmission through the earshell for the inertial actuator configuration as simulated from the measured data, before and after the control force is applied. The notch at around 250 Hz is due to the mounting of the actuator system acting as a tuned neutralizer. The control filter was designed to provide best attenuation at the frequency range of 250–600 Hz, therefore attenuating the resonance of the mounted system. An attenuation of up to 20 dB is achieved in the control frequency range, showing potential for good performance in practice. A slight increase in the sound transmission is observed at the low frequencies, which is in line with the results predicted in the model-based simulations presented in Fig. 6(a). It should be noted that the curve denoted "Active OFF" in Fig. 11(a), which represents passive transmission, is different from the curve denoted "Data" in Fig. 4, which also represents passive attenuation, in two aspects. First, the former includes the effect of the mounted actuator, and second, the latter was taken from manufacturer's data, while the former was measured on the laboratory headset system used in this work. These two factors contributed to the dissimilarity between the two passive transmission curves.

Figure 11(b) shows the Nyquist plot of the open-loop response CH for the measured plant H and the feedback controller C designed above. The controller maintains reasonable margins from the instability point $(-1,0)$, while achieving an open-loop gain of about 10 on the positive-real quadrant.

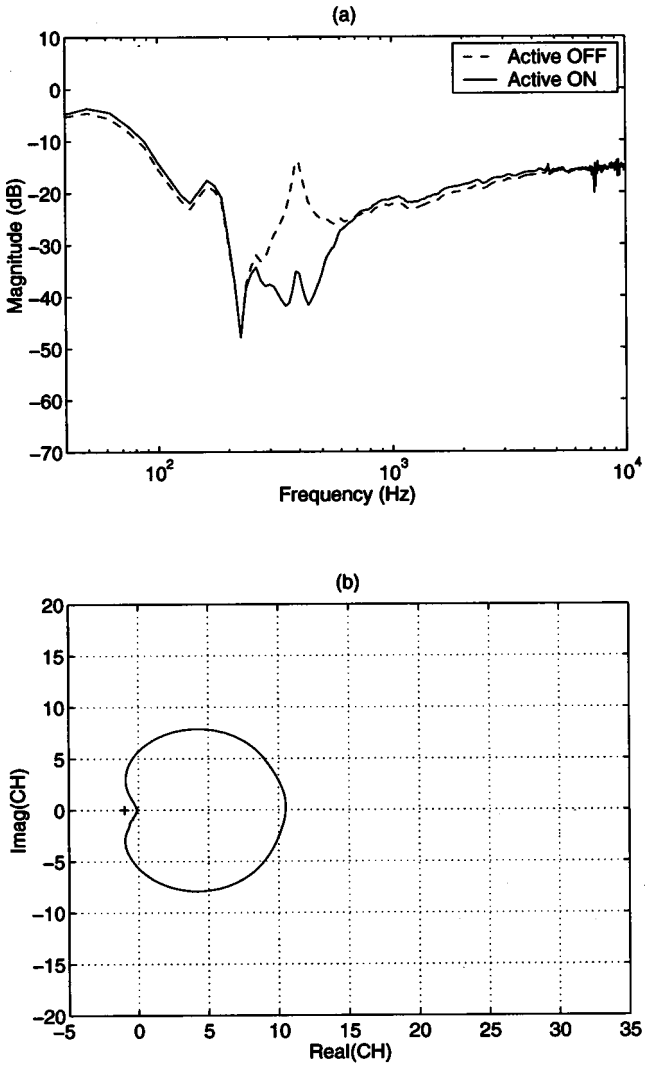

FIG. 11. (a) Sound transmission simulated from measured data for the inertial control actuator configuration, and (b) the corresponding Nyquist diagram of the open-loop response of the active system.

C. Control with headband force actuator

A laboratory headset system with the actuator placed between the headband and the earshell was constructed as described above, and performance was investigated through control simulations from measured data. As for the inertial actuator configuration, velocity feedback control produced poor performance due to high-frequency dynamics, and so a control filter C was designed as described above with a control bandwidth that includes the frequencies below 800 Hz. Figure 12(a) show the sound transmission simulated from measured data before and after control. Attenuation of up to 10 dB is achieved in this broadband control bandwidth. Note that the sound transmission at low frequencies is higher than expected, which can be explained by imperfect sealing of the headset in the experimental setup. Figure 12(b) presents the Nyquist plot of the open-loop response, showing that good

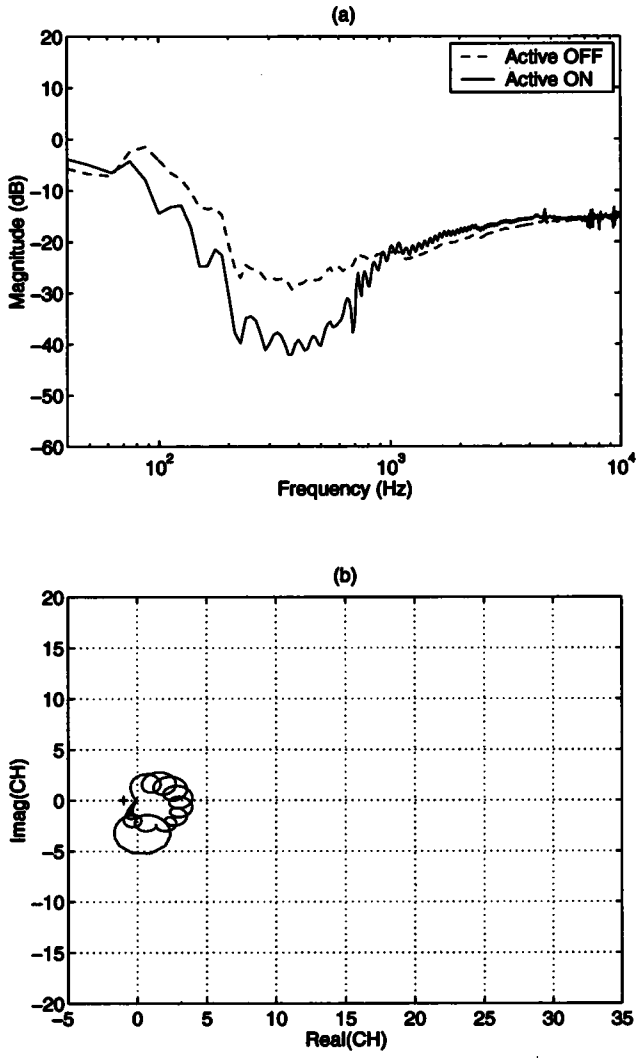

FIG. 12. (a) Sound transmission simulated from measured data for the headband control actuator configuration, and (b) the corresponding Nyquist diagram of the open-loop response of the active system.

stability margins are achieved with a maximum open-loop gain of about 5. The results presented here also show potential for useful performance in practice.

It should be noted that the potential delay of a digital controller originating from the sampling process and the low-pass filters was not considered in the performance analysis in this work. The predicted performance may therefore be achieved by a digital system with a high sampling rate and therefore small delay, or an analog system with a similar frequency response. Although the design of such broadband real-time controllers is suggested for future work, a single-frequency real-time control system was designed and implemented, and is presented below.

V. REAL-TIME CONTROL EXPERIMENT

A real-time control experiment was performed in which single-frequency tonal noise was attenuated by the laboratory headset system with the actuator attached to the headband. A digital controller was designed which implemented a finite impulse response (FIR) control filter having 128 coefficients, adapted using the LMS algorithm,[20] and an FIR plant model

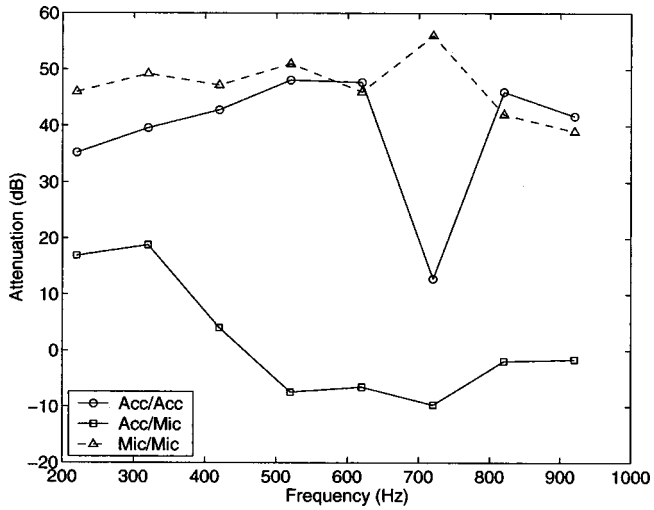

FIG. 13. Single frequency attenuation in the real-time control experiment, when the accelerometer was used for both control and attenuation measurement (Acc/Acc); when the accelerometer was used for control but the microphone used for the attenuation measurement (Acc/Mic); and when the microphone was used for both control and attenuation measurement (Mic/Mic).

of the same length. Both filters were part of an IMC controller[21] operating at a sampling frequency of 5 kHz. A system identification routine based on the LMS algorithm[20] was initiated first to calculate the value of the plant model filter, after which the primary source was turned on, and the control filter adapted to minimize the mean-squared sensor signal. Once the control filter converged, the level of the signal at the sensor was measured and compared to its level before control, giving the attenuation due to the active control system.

Due to the relatively large delay of the adaptive system, based on a Texas Instruments TMS320C54x DSP kit, the performance was limited to narrow-band or tonal disturbances. For this reason the broadband controllers designed in Sec. IV could not be successfully implemented in real time using the current DSP system, and so performance was studied using single-frequency tones, and an LMS-based adaptive control system, which is well suited to control such disturbance. Nevertheless, the real-time experiment presented below showed that indeed active control can be performed using force actuators mounted on the headset earshell as suggested in this paper. The experiment also provides an interesting comparison of performance when the sensing transducer is either an accelerometer or a microphone.

An experimental setup similar to that described in Sec. IV was used in the real-time control experiment. In addition, the output of the DSP controller was connected to the actuator amplifier, while the input of the DSP controller was connected to the output of the sensor, which was either the accelerometer or the microphone inside the earshell. A loudspeaker positioned near the headset setup was used to generate the primary excitation.

Figure 13 (the two solid curves) shows the attenuation at the tonal excitation frequencies as measured by the accelerometer, mounted opposite the force acuator, in a colocated manner, and the microphone. In this case the accelerometer

was used as the control sensor, such that the control filter attempted to minimize the mean-square error of the accelerometer signal. Although large attenuation is achieved at the control sensor, an attenuation of more than 10 dB at the microphone is only achieved at the low frequencies, and in fact at high frequencies the noise is actually amplified.

This behavior can be explained by the fact that although the vibration of the earshell is reduced at the accelerometer location, other parts of the earshell could still vibrate by exciting higher-order modes, specially at high frequencies, therefore radiating sound into the earshell inner volume. Another contributing factor for this behavior could be transmission paths other than via earshell vibration, such as acoustic leaks, which are not eliminated by reducing headset vibration.

A second experiment was performed, this time with the microphone as the control sensor. As can be seen from Fig. 13 (dashed curve), high attenuation is achieved at a wide frequency range. In this case the controller is attempting to minimize the microphone signal directly, and so rather then reducing the earshell vibration, the actuator forces the earshell to vibrate in such a way that minimizes the sound level inside the earshell, therefore overcoming the potential problems when minimizing the vibration signal as discussed above.

The results presented here suggest that a microphone can be more useful as a control sensor since it measures the sound inside the earshel directly. Measuring the sound indirectly, using an accelerometer mounted on the earshell, results in reduction in the earshell vibration, but due to high-frequency dynamics and leaks, this reduction might not produce as significant a reduction in the sound. The microphone control sensor could therefore provide a more attractive alternative for a practical active headset system.

VI. CONCLUSIONS

This paper presented a novel approach to ANR headsets, which employ earshell vibration control to attenuate the noise inside the earshell volume. The theory of the new approach, supported by simulations and an experimental study, suggested that good performance can potentially be achieved in practice.

Two actuator configurations were studied, i.e., an inertial force actuator and a force actuator placed between the earshell and the headband. Model-based simulations highlighted the requirement for a reduced stiffness from the actuator, and provided actuator's force and stroke requirements, while simulations from data measured on a laboratory headset system showed that good performance could potentially be achieved.

The configuration with a force actuator placed between the headband and the earshell is preferred since it doesn't require an inertial mass which will increase system weight and compromise comfort. Furthermore, the piezoelectric actuator considered here requires high-input voltage, which might be difficult to obtain in a commercial active headset.

Another important issue is the effect of leaks caused by an imperfect seal of the headset to the head and the effect of high-frequency system dynamics. The use of a microphone rather than an accelerometer which will detect noise generated by both vibration transmission and sound leak paths was shown to be preferable, through a single-frequency real-time control experiment.

The study and design of more suitable actuators and their implementation in an active noise-reducing headset are proposed for future research. The subjective effect of noise reduction through earshell vibration should also be investigated as sound might be perceived via bone conduction. Another important issue is the mechanical coupling between left and right headset systems via the headband, for example, which should be investigated and be taken into account if found significant.

ACKNOWLEDGMENTS

The authors would like to thank Lectret Precision Pte. Ltd. for supporting the research work.

[1] E. D. Simshauser and M. E. Hawley, ''The noise canceling headset—An active ear defender,'' J. Acoust. Soc. Am. **27**, 207 (1955).
[2] M. H. Hawley, ''Acoustic interference for noise control,'' Noise Control **2**, 61–63 (1956).
[3] W. F. Meeker, ''Components characteristics for an active ear defender,'' J. Acoust. Soc. Am. **29**, 1252 (1957).
[4] P. D. Weeler, ''Voice communication in the cockpit noise environment,'' Ph.D. thesis, University of Southampton, England, 1986.
[5] M. S. Bai and D. Lee, ''Implementation of an active headset by using H_∞ robust control theory,'' J. Acoust. Soc. Am. **102**, 2184–2190 (1997).
[6] A. J. Brammer, G. J. Pan, and R. B. Crabtree, ''Adaptive feedforward active noise reduction headset for low-frequency noise,'' Proceedings of ACTIVE 97 conference, Budapest, Hungary, August 1997, pp. 365–372.
[7] A. V. Oppenheim, E. Weinstien, K. C. Zangi, M. Feder, and D. Gauger, ''Single-sensor active noise cancellation,'' IEEE Trans. Audio Speech Proc. **2**(2), 285–290 (1994).
[8] B. Rafaely and M. Jones, ''Combined feedback-feedforward active noise-reducing headset—The effect of acoustics on broadband performance,'' J. Acoust. Soc. Am. (in press).
[9] B. Rafaely, P. Gardonio, and J. Carhillo, ''Novel active headset,'' Patent GB2361379.
[10] E. A. G. Shaw and G. J. Thiessen, ''Acoustics of circumaural earphones,'' J. Acoust. Soc. Am. **34**, 1233–1246 (1962).
[11] C. R. Fuller, S. J. Elliott, and P. A. Nelson, *Active Control of Vibration* (Academic, London, 1997).
[12] P. A. Nelson and S. J. Elliott, *Active Control of Sound* (Academic, London, 1992).
[13] C. M. Harris and C. E. Crede, *Shock and Vibration Handbook* (McGraw-Hill, New York, 1976).
[14] S. J. Elliott, M. Serrand, and P. Gardonio, ''Feedback stability for active isolation systems with reactive and inertial actuators,'' ASME J. Vibr. Acoust. **123**(2), 250–261 (2001).
[15] M. J. Brennan, J. Garcia-Bonito, S. J. Elliott, A. David, and R. J. Pinnington, ''Experimental investigation of different actuator technologies for active vibration control,'' Smart Mater. Struct. **8**, 145–153 (1999).
[16] M. Morari and E. Zafiriou, *Robust Process Control* (Prentice-Hall, Englewood Cliffs, NJ, 1989).
[17] B. Rafaely and S. J. Elliott, ''H_2/H_∞ active control of sound in a headrest: Design and implementation,'' IEEE Trans. Control Syst. Technol. **7**(1), 79–84 (1999).
[18] S. J. Elliott and T. J. Sutton, ''Performance of feedback and feedforward systems for active control,'' IEEE Trans. Speech Audio Proc. **4**(3), 214–223 (1996).
[19] M. S. Bai and D. Lee, ''Implementation of an active headset by using H-infinity robust control theory,'' J. Acoust. Soc. Am. **102**, 2184–2190 (1997).
[20] B. Widrow and S. D. Stearns, *Adaptive Signal Processing* (Prentice-Hall, Englewood Cliffs, NJ, 1985).
[21] B. Rafaely and S. J. Elliott, ''An adaptive and robust feedback controller for active control of sound and vibration,'' Proceedings of CONTROL'96 conference, University of Exeter, UK, 1996, pp. 1149–1153.